

Supervised Training of Neural-Network Quantum States for the Next-Nearest Neighbor Ising Model

Zheyu Wu^{a,1}, Remmy Zen^{b,1}, Heitor P. Casagrande^a, Dario Poletti^{a,c,d,e,2},
Stéphane Bressan^f

^a*Science, Mathematics and Technology Cluster, Singapore University of Technology and
Design, 8 Somapah Road, 487372, Singapore, Singapore*

^b*Max Planck Institute for the Science of Light, Staudtstraße
2, 91058, Erlangen, Germany*

^c*Engineering Product Development Pillar, Singapore University of Technology and
Design, 487372, Singapore, Singapore*

^d*Centre for Quantum Technologies, National University of Singapore, 3 Science Drive
2, 117543, Singapore, Singapore*

^e*MajuLab, CNRS-UCA-SU-NUS-NTU International Joint Research Unit, Radarweg
29, 1043 NX, Singapore, Singapore*

^f*School of Computing, National University of Singapore, 13 Computing
Drive, 117417, Singapore, Singapore*

Abstract

Different neural network architectures can be unsupervisedly or supervisedly trained to represent quantum states. We explore and compare different strategies for the supervised training of feed forward neural network quantum states. We empirically and comparatively evaluate the performance of feed forward neural network quantum states in different phases of matter for variants of the architecture, for different hyper-parameters, and for two different loss functions, to which we refer as *mean-squared error* and *overlap*, respectively. We consider the next-nearest neighbor Ising model for the diversity of its phases and focus on its paramagnetic, ferromagnetic, and pair-antiferromagnetic phases. We observe that the overlap loss function allows better training of the model across all phases, provided a rescaling of the neural network.

¹These authors contributed equally to this work.

²dario_poletti@sutd.edu.sg to whom correspondence should be sent

1. Introduction

Machine learning models, in general [1–6], and neural networks, in particular, have been used in a variety of applications including phase characterization [7–9], experimental guidance [10], state tomography [11–17], process tomography [18, 19], control [20–22], the learning of Hamiltonians [23–27] and dissipators [28, 29], and the learning of wave functions for both equilibrium and non-equilibrium cases [30–49].

In the latter application, *neural-network quantum states*, originally proposed in Ref. [30], refer to a family of neural networks trained to approximate the wave function of a quantum system, namely to return unnormalized probability or the probability amplitude corresponding to each configuration of the quantum system.

Numerical methods to study quantum systems face the challenge that the Hilbert space size increases exponentially with the number of components. It is not possible for any method on a classical computer to describe all the possible wave functions. However, one can search for methods to accurately describe physically relevant states. In this work, we focus on ground states of the one-dimensional next-nearest neighbor quantum Ising model because the ground state can be in four different phases: paramagnetic, ferromagnetic, antiferromagnetic, and pair-antiferromagnetic phases. While the classical Ising model has already been investigated with the use of neural networks [50–52], the quantum Ising model with next-nearest neighbor couplings is more complex and requires deeper investigations. An important point in the use of neural network is its trainability. Even if a network could represent a certain wave function or probability distribution, it may not be effective or efficient to train it to reach that goal function. Here, in particular, we wonder, within the same structure of the neural network, which optimization routines can allow us to describe accurately the very different phases of these ground states.

Neural-network quantum states can be unsupervisedly or supervisedly trained. Unsupervised neural-network quantum states, for instance, variationally optimize the model parameters to minimize the energy of a system [30]. Unsupervised learning is frequently performed by stochastic reconfiguration [53], and can be accelerated by transfer learning [41, 42], sequential local optimization [54] or by computing the geometric tensor on the fly [55].

Supervised neural-network quantum states are trained with a (large) corpus of configurations and their probabilities or probability amplitudes [8]

obtained from other numerical simulations or, more importantly, from experiments. Supervised learning has two main applications. Firstly, it reveals whether a particular model is expressive enough and sufficiently easily trainable to represent a specific wave function in practice. This information can then be used to select that model to describe similar systems or classify the types of physical systems and correlations that the machine learning model can describe. Secondly, it yields a machine representation of the wave function that can further be used to compute additional elements and gather insights into the physical system, which may otherwise be challenging to obtain experimentally. For instance, not all observables (e.g. long-range correlations) and measurables (e.g. entropy and out-of-time-ordered correlators [56]) are readily accessible on experimental platforms.

To gain general strategies on how to effectively perform supervised learning, here we explore and compare different strategies for the supervised training of a neural-network quantum states architecture consisting of a feed forward neural network. We comparatively evaluate the performance, namely the effectiveness of the training, of feed forward neural network quantum states in different phases of matter for variants of the architecture, for instance, different number of hidden nodes, for different hyper-parameters, different learning rates, and different number of samples. In particular, we consider two different loss functions, to which we refer as *mean-squared error* and *overlap*, respectively.

As we mentioned before, we consider the one-dimensional next-nearest neighbor quantum Ising model. What is important to add here is that this model also has the advantage that it can be studied very accurately and efficiently using matrix product state algorithms [57]. We will thus use this algorithm to produce the exact ground state from which we will also sample the configurations and thus provide the data to train the neural networks. This will allow us to effectively study the expressive power of the networks and the possibility of training them.

The paper is structured as follows. Section 2 introduces the neural network architecture, the supervised training, and the two loss functions considered. Section 3 describes the physical system studied and recalls its properties. Section 5 presents and analyzes the results of the comparative empirical evaluation. Finally, Section 6 summarizes the findings.

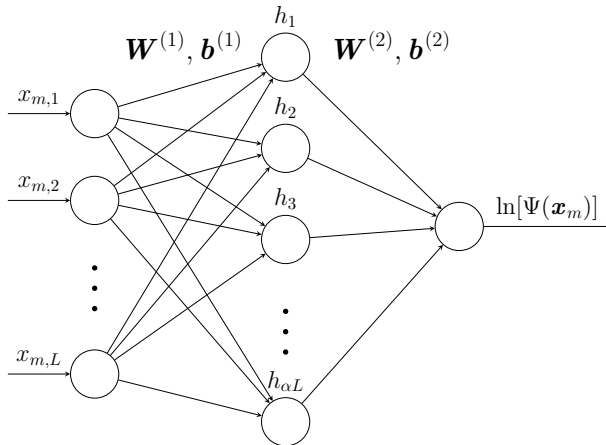


Figure 1: Feed forward neural network architecture. Inputs are $x_{m,i}$, the elements of a spin configuration \mathbf{x}_m , L is the number of spins of the system, with one hidden layer of size αL and output $\ln[\Psi(\mathbf{x}_m)]$. W and b are the weights and biases, respectively.

2. Supervised neural-network quantum states

Neural-network quantum states belong to the family of variational Monte Carlo methods and use neural networks as the trial wave function. They were proposed by the authors of [30] to represent with a neural network the amplitude $\Psi(\mathbf{x}_m)$ of the configurations \mathbf{x}_m of a quantum state. Here, our choice of the neural network is a feed forward neural network, where each visible node represents one of the L particles of the quantum many-body system. More specifically, a visible node can take the values -1 or 1 depending on whether the spin at that location is pointing down or up, respectively. Figure 1 depicts a feed forward neural network with a single hidden layer. Note that the output layer returns the natural logarithm of the probability amplitude associated with one configuration, i.e. $\ln[\Psi(\mathbf{x}_m)]$, because the wave function typically takes values that vary over different orders of magnitude. One advantage of a feed forward neural network is its flexible design and easier to construct deeper structure.

In feed forward neural-network quantum states, we use a concatenation of linear and nonlinear functions given by

$$\ln[\Psi(\mathbf{x}_m)] = \sigma^{(k)}(\mathbf{W}^{(k)} \dots \sigma^{(1)}(\mathbf{W}^{(1)} \mathbf{x}_m + \mathbf{b}^{(1)}) \dots + \mathbf{b}^{(l)}), \quad (1)$$

where $\mathbf{W}^{(k)} \mathbf{x}_m + \mathbf{b}^{(k)}$ is the linear part at layer k , $\mathbf{W}^{(k)}$ and $\mathbf{b}^{(k)}$ represent the neural network parameters at layer k . $\mathbf{W}^{(k)}$ are the parameters which

fully connect the nodes between adjacent layers and $\mathbf{b}^{(k)}$ are the bias. While $\sigma^{(k)}$ is the nonlinear activation function at layer k . For our purpose, it is sufficient to consider a single hidden layer. The number of nodes in this layer is given by αL . We refer to α as the hidden ratio. For the activation function $\sigma^{(k)}$, for $k = 1$ we use leaky ReLU [58], which is given by

$$\text{LeakyReLU}(x) = \begin{cases} x & \text{if } x \geq 0 \\ \eta x & \text{otherwise} \end{cases} \quad (2)$$

where η is a constant we choose to fix it to 0.01 for our experiments. This activation function can prevent vanishing gradient, which could happen with ReLU performing on negative input.

The supervised training of neural-network quantum states is analogous to the regression problem in standard machine-learning settings. We used labeled data $(\mathbf{x}_m, \ln[\Psi_G(\mathbf{x}_m)])$ pairs, where $\Psi_G(\mathbf{x}_m)$ is the exact value of probability amplitude for the spin configuration \mathbf{x}_m . Here m goes from 1 to M , while M_u is the number of unique samples, as sometimes many configurations could be repeated. The samples should be representative of the probability distribution stemming from the wave function, and they could come from experimental data, although, here, we use numerically generated ones. In the following, we also use the notation $\ln[\tilde{\Psi}(\mathbf{x}_m)]$ for the rescaled output of the neural network, which is given by

$$\ln[\tilde{\Psi}(\mathbf{x}_m)] = \frac{\ln[\Psi(\mathbf{x}_m)]}{\max_k \ln[\Psi(\mathbf{x}_k)]}, \quad k \in [1, M_u] \quad (3)$$

which is the output of the neural network divided by the maximum occurring for the configurations considered. From this it follows that

$$\tilde{\Psi}(\mathbf{x}_m) = \exp[\ln[\tilde{\Psi}(\mathbf{x}_m)]]. \quad (4)$$

To obtain $\Psi_G(\mathbf{x}_m)$, we use a matrix product state algorithm with the zipper method to obtain the samples [59–61]. While the total size of the possible labeled data is 2^L , where L is the size of the system under study, in general, we can only take a much smaller number of sample M drawn from the distribution $|\Psi_G(\mathbf{x}_m)|^2$ using the Metropolis-Hastings algorithm [62, 63].

Among the variety of possible loss functions, we consider minimizing two different possible loss functions to train the neural network: the mean-squared error (MSE) which is commonly used to conduct supervised learning,

given by

$$\mathcal{L}_{\text{MSE}}(\Psi_G, \Psi) = \frac{1}{M} \sum_{m=1}^M \left(\ln [\Psi_G(\mathbf{x}_m)] - \ln [\Psi(\mathbf{x}_m)] \right)^2, \quad (5)$$

and the overlap between two wave functions, given by

$$\mathcal{L}_{\text{Overlap}}(\Psi_G, \tilde{\Psi}) = -\ln \left[\frac{\langle \Psi_G | \tilde{\Psi} \rangle \langle \tilde{\Psi} | \Psi_G \rangle}{\langle \Psi_G | \Psi_G \rangle \langle \tilde{\Psi} | \tilde{\Psi} \rangle} \right]. \quad (6)$$

We note that, in Equation (6), we can rewrite each term according to

$$\langle \Psi_A | \Psi_B \rangle = \sum_{m=1}^{M_u} \Psi_A^*(\mathbf{x}_m) \Psi_B(\mathbf{x}_m). \quad (7)$$

This is also used in Ref. [64]. Here we used $\tilde{\Psi}_\beta(\mathbf{x}_m)$, where $\beta = A, B, \dots$, and not $\Psi_\beta(\mathbf{x}_m)$ because we need to exponentiate the output of the neural network and this can lead to instabilities, see Ref. [55] and [Appendix A](#). Note that in Equation (6-7), we use the unique samples M_u instead of all the samples. This is because in the calculation of the overlap there is already the probability of each unique samples, and if we were to take all the samples into account (with repetitions proportional to the probability), the probability of the samples would be weighted twice. As a result, the normalization would be skewed towards the more probable configurations³. We then compute the gradient of the loss functions and update the parameters using an initial learning rate γ and Adam optimizer introduced in Ref. [65].⁴

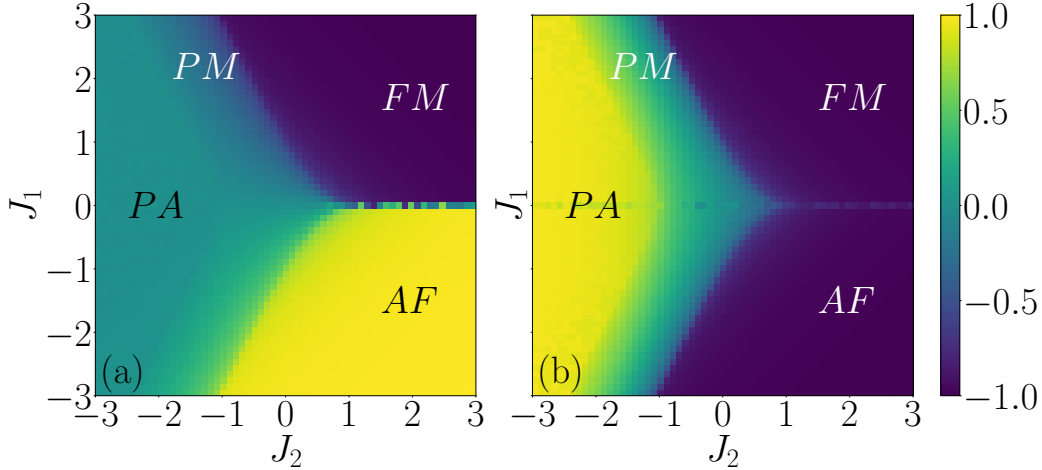


Figure 2: Phase diagram of the next-nearest neighbor Ising model, Equation (9) with $h_x = 1$ and system size $L = 128$, in terms of tunneling J_1 and J_2 interactions. (a) Nearest-neighbor correlation C_{NN} from Equation (10); (b) Next-nearest neighbor correlation C_{NNN} from Equation (11). Paramagnetic region is labeled by PM , ferromagnetic by FM , antiferromagnetic by AF , and pair-antiferromagnetic by PA .

3. The next-nearest neighbor Ising model

While supervised training can, in principle, be used to learn any state, we focus on training ground states with different properties. The main reason why we use ground states is that with the methods we use to generate data, i.e. matrix product states, ground states can be efficiently and effectively produced [66]. As for the physical model studied, for our analysis, we choose the next-nearest neighbor Ising model because its ground state can be in four

³Note that one could use unique samples also for the MSE loss function by slightly modifying it to

$$\mathcal{L}_{\text{MSE}}(\Psi_G, \Psi) = \sum_{m=1}^{M_u} |\Psi_G(\mathbf{x}_m)|^2 \left(\ln[\Psi_G(\mathbf{x}_m)] - \ln[\Psi(\mathbf{x}_m)] \right)^2. \quad (8)$$

However, in our empirical evaluations, we find that the loss function which considers all the samples has a more consistent response. This could be investigated further in future works.

⁴In the initialization of the neural network, and generation of the batches, we use the same random seed for different numerical experiments.

different phases. More specifically, the Hamiltonian is given by

$$H = -h_x \sum_{l=1}^L \sigma_l^x - J_1 \sum_{l=1}^L \sigma_l^z \sigma_{l+1}^z - J_2 \sum_{l=1}^L \sigma_l^z \sigma_{l+2}^z, \quad (9)$$

where σ_l^a are the corresponding Pauli matrices (with $a = x, y, z$) at site l , h_x is the magnetic field along the x axis, and J_1 and J_2 are nearest neighbor and next-nearest neighbor couplings, respectively. We note that the Hamiltonian has a ‘‘particle-hole’’ symmetry such that one can map a Hamiltonian with coupling J_1 to one with coupling $-J_1$ via the operator $S = \prod_j \sigma_{2j}^x$, i.e. $H(J_1) = SH(-J_1)S^\dagger$. This transformation, for instance, turns a ferromagnetic phase into an antiferromagnetic phase. It is thus sufficient to study the system for positive values of J_1 . The phase diagram, in terms of J_1 and J_2 , is depicted in Figure 2 for $L = 128$ and $h_x = 1$, which is the energy scale we use throughout the paper. To compute the ground state from which to obtain the training data, we have used a matrix product states code built using ITENSOR libraries [67, 68]. To identify the phases we use the nearest-neighbor ferromagnetic correlator C_{NN} given by

$$C_{NN} = -\frac{1}{L-1} \sum_{l=1}^{L-1} \sigma_l^z \sigma_{l+1}^z, \quad (10)$$

depicted in Figure 2(a), and the next-nearest neighbor antiferromagnetic correlator $C_{N NN}$, given by

$$C_{N NN} = \frac{1}{L-2} \sum_{l=1}^{L-2} \sigma_l^z \sigma_{l+2}^z, \quad (11)$$

shown in Figure 2(b).

In the ferromagnetic phase, C_{NN} and $C_{N NN}$ are both large and negative. In the pair-antiferromagnetic phase, e.g. spin configurations of the type $\uparrow\uparrow\downarrow\downarrow\uparrow\uparrow\downarrow\downarrow$, only $C_{N NN}$ is large and positive while C_{NN} approaches zero. The paramagnetic phase is located between these two phases, for which both order parameters are small⁵. For negative J_1 , we can obtain the possible phases by

⁵Along the line $J_1 = 0$ we have a pixelated region which is due to the small energy gap and the significant difference in properties of the lowest energy eigenstates. We note that we did not use data for $J_1 = 0$ to train the neural network.

applying the operator S , resulting in an antiferromagnetic phase and another pair-antiferromagnetic phase, separated by a paramagnetic phase. We also note that for $J_1 > 0$, the probability amplitude $\Psi(\mathbf{x}_m)$ can be written as a positive real number. Thus one can use a feed forward neural network model with real weights and biases without complex numbers.

4. The Mapalus Library

Carleo et al. presented the first open-source library for neural-network quantum states, called NETKET, in [69]. Initially, the core of NETKET was implemented in C++ with an interface to Python. However, it is now a Python library that uses the JAX library [70] to support general-purpose graphics processing units.

We developed a library, called MAPALUS, that implements neural-network quantum states with the TENSORFLOW library [71]. We choose TENSORFLOW over other deep learning frameworks for its widespread use [72] and user-friendly application programming interface. MAPALUS is available at <https://github.com/remmyzen/mapalus> and is the library used in this work. See Appendix C for more details.

5. Results

In this section, we study the performance of training the feed forward neural network. We consider a large system with $L = 128$ in three different phases namely the paramagnetic phase, the ferromagnetic phase, and the pair-antiferromagnetic phase. We comparatively evaluate the performance for the two different loss functions $\mathcal{L}_{\text{Overlap}}$ and \mathcal{L}_{MSE} together with various training parameters. One important training parameter is the number of training samples M , which, if not stated otherwise, we set to 10^5 . For $\mathcal{L}_{\text{Overlap}}$, we first obtain the M samples, then only use the corresponding M_u unique ones to update the neural network. During the training, we typically only use a portion of these data to evaluate the loss function and optimize the parameters at each epoch. We call the number of samples in this portion of the data as *batch size* and refer to it with the symbol B , which, if not stated otherwise, we set to $B = 32$. Another parameter we vary is the hidden ratio α , which, if not stated otherwise, we set to $\alpha = 3$.

To evaluate the effectiveness of the training, we study the relative energy error \mathcal{E}_r defined by

$$\mathcal{E}_r = \left| \frac{E_T - E_G}{E_G} \right|, \quad (12)$$

where E_G is the ground state energy computed from matrix product states simulations, while E_T is the energy of the trained wave function. For the trained wave function, we evaluate the energy by

$$E_T = \frac{1}{M} \sum_{m=1}^M E_{\text{loc}}(\mathbf{x}_m) \quad (13)$$

when using \mathcal{L}_{MSE} , as we use all the M samples, and

$$E_T = \sum_{m=1}^{M_u} |\Psi(\mathbf{x}_m)|^2 E_{\text{loc}}(\mathbf{x}_m) \quad (14)$$

when using $\mathcal{L}_{\text{Overlap}}$ because it uses only the unique samples M_u .

In Equations (13) and (14), the so-called local energy, local in the sense of configurations, E_{loc} is given by

$$E_{\text{loc}}(\mathbf{x}_m) = \sum_{m'} H_{m',m} \frac{\Psi(\mathbf{x}_{m'})}{\Psi(\mathbf{x}_m)}, \quad (15)$$

where $H_{m',m}$ is the matrix element of the Hamiltonian which connects the two configurations \mathbf{x}_m and $\mathbf{x}_{m'}$. Naturally, if we already knew what the Hamiltonian was, we could have done the unsupervised training, but here we use the Hamiltonian to compute a ground truth reference and quantify the effectiveness of the method.

5.1. Training in the paramagnetic phase

The results for the paramagnetic phase are shown in Figure 3. In Figure 3(a,c,e), we show results for the loss function $\mathcal{L}_{\text{Overlap}}$, while in panels (b,d,f) we have considered \mathcal{L}_{MSE} . In panels (a) and (b) we keep all parameters as default values mentioned earlier except for the batch size B , in panels (c) and (d) we vary the number of samples M , and in panels (e) and (f) we consider different hidden ratios α . Here, the parameters in Hamiltonian are $J_1 = 2$ and $J_2 = -1$, and we have used an initial learning rate $\gamma = 10^{-5}$.

The default parameters, unless stated otherwise, are the number of samples $M = 10^5$, batch size $B = 32$, and hidden ratio $\alpha = 3$.

In all panels, we look at the relative error of the energy \mathcal{E}_r versus the number of epochs E . We observe that both loss functions allow reaching low relative errors of the order of 10^{-2} .⁶ In general, both a smaller batch size (see [Appendix B](#)), and a larger number of samples result in better accuracy. Furthermore, for both loss functions, a larger hidden ratio can also result in better accuracy.

5.2. Training in the ferromagnetic phase

We consider the ferromagnetic phase, for Hamiltonian parameters $J_1 = 1$ and $J_2 = 2$. The default values, unless otherwise stated, are $M = 10^5$ for the number of samples, $\alpha = 3$ for the hidden ratio, $B = 32$ for the batch size, and $\gamma = 10^{-5}$ for the initial learning rate. The results are shown in [Figure 4](#), in a similar structure as in [Figure 3](#).

In [Figure 4](#), we observe that in some cases, the error becomes very small, and then it increases. This is due to the fact that in those cases, the energy E_T obtained from training the neural network starts from below the ground state value, then goes above it, and then may decrease again when approaching the exact value from above. We point out that this is not at odds with the variational principle, for which the energy is bounded from below compared to that of the ground state. This is because, when sampling, we may not evaluate the Hamiltonian correctly and it is thus possible to estimate an energy value lower than the exact ground state energy. Overall, in the ferromagnetic phase, we observe a similar behavior as with the paramagnetic phase. However, we can reach more accurate predictions of the energy with a relative error of the order of 10^{-3} or even smaller. Smaller batch sizes are generally helpful for both loss functions, and so are more number of samples, while a larger number of hidden nodes seems to lead to overfitting for $\mathcal{L}_{\text{Overlap}}$, [Figure 4\(e\)](#), while it still allows (marginal) improvements for \mathcal{L}_{MSE} , [Figure 4\(f\)](#). We associate this overfitting to the relative simplicity of the wave function to be described by the network. We still observe that $\mathcal{L}_{\text{Overlap}}$ allows the energies to reach values closer to the ground state energy.

⁶When using an initial learning rate $\gamma = 10^{-4}$, with $\mathcal{L}_{\text{Overlap}}$ it is possible to reach even better accuracy of the energy, however, the learning dynamics is more involved (not shown). Using \mathcal{L}_{MSE} instead, the prediction of the ground state energy does not improve significantly.

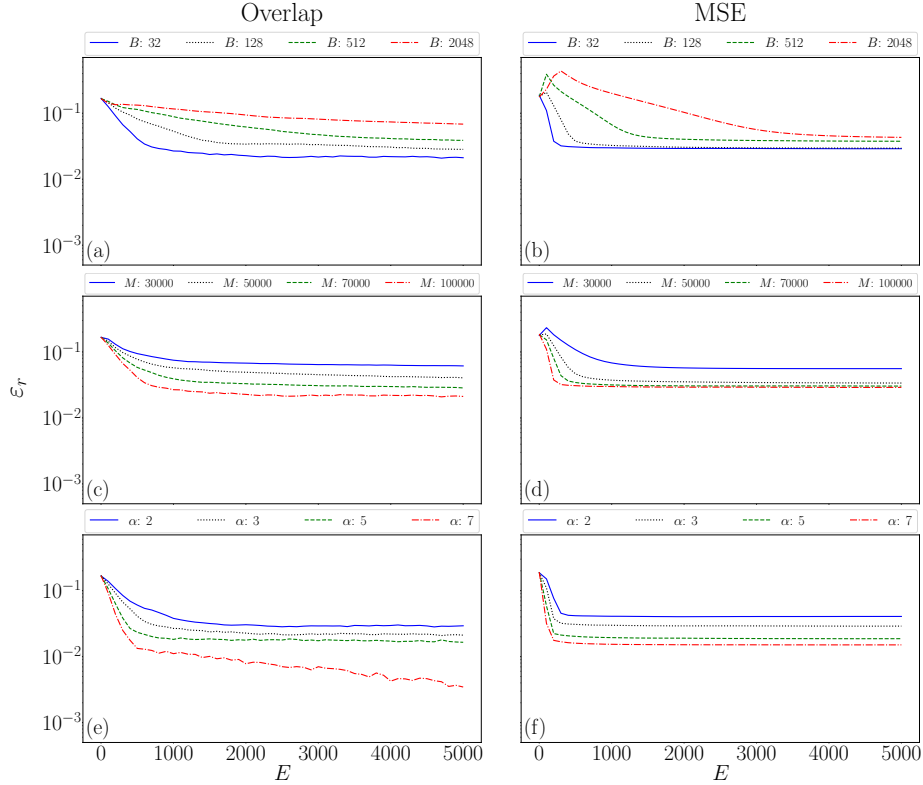


Figure 3: Relative error \mathcal{E}_r for the paramagnetic ground state ($J_1 = 2$ and $J_2 = -1$) versus the number of epochs E . In panels (a, c, e), we use overlap loss function $\mathcal{L}_{\text{Overlap}}$; in panels (b, d, f), we use \mathcal{L}_{MSE} . In panels (a,b), we vary the batch size B . In panels (c,d), we vary the number of samples M ; in panels (e,f), we vary the hidden ratio α . If not stated otherwise, the number of training samples is $M = 10^5$, the hidden ratio is $\alpha = 3$, the batch size is $B = 32$ and $\gamma = 10^{-5}$ is the initial learning rate.

5.3. Training in the pair-antiferromagnetic phase

In the pair-antiferromagnetic phase, for $J_1 = 1$ and $J_2 = -2$, we presented the results in Figure 5 following the same structure as Figure 3 and Figure 4. The default values of the training parameters are $M = 10^5$ for the number of samples, $\alpha = 3$ for the hidden ratio, $B = 32$ for the batch size, and $\gamma = 10^{-5}$ for the initial learning rate. The shown curves result from the fact that the initial energy of the state is below the ground state energy, and that it requires a larger number of epochs to approach the ground state. We computed 10^4 epochs here as the model has slower optimization dynamics. In general, we still observe some form of overfitting for $\mathcal{L}_{\text{Overlap}}$, Figure 5(e),

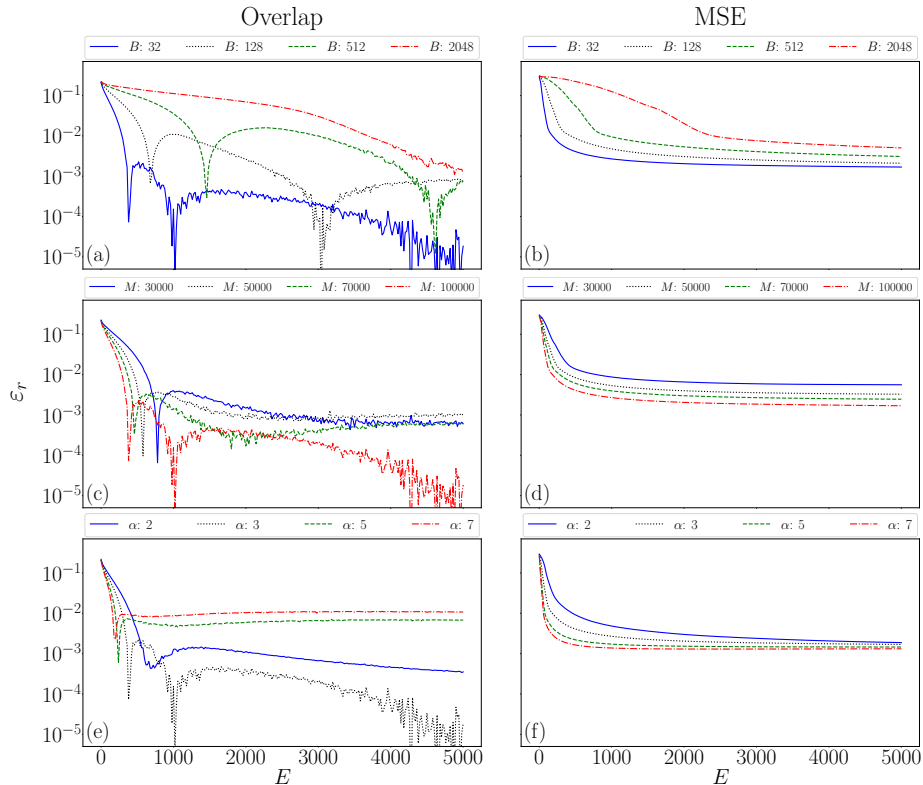


Figure 4: Relative error \mathcal{E}_r for the ferromagnetic ground state ($J_1 = 1$ and $J_2 = 2$) versus the number of epochs E . In panels (a, c, e), we use overlap loss function $\mathcal{L}_{\text{Overlap}}$; in panels (b, d, f), we use \mathcal{L}_{MSE} . In panels (a,b), we vary the batch size B . In panels (c,d), we vary the number of samples M ; in panels (e,f), we vary the hidden ratio α . If not stated otherwise, the number of training samples is $M = 10^5$, the hidden ratio is $\alpha = 3$, the batch size is $B = 32$ and $\gamma = 10^{-5}$ is the initial learning rate.

and a general improvement of performance with an increasing number of samples M , Figure 5(c,d). As for the batch size, a smaller batch size results in approaching the ground state energy in a smaller number of epochs, see Figure 5(a,b).

5.4. Convergence of loss function and relative energy error

In supervised training one typically only has access to data such as configurations and their corresponding probability amplitude, and not to the Hamiltonian of the system. During the training, we can monitor the evolution of the loss function, but this does not directly imply that other properties

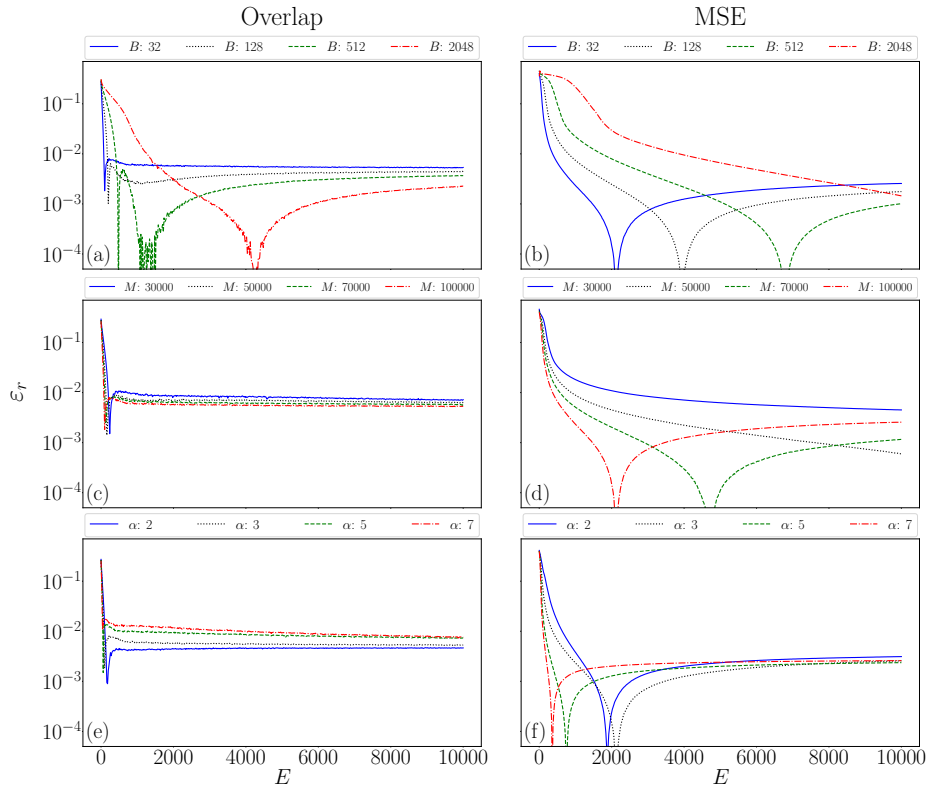


Figure 5: Relative error \mathcal{E}_r for the pair-antiferromagnetic ground state ($J_1 = 1$ and $J_2 = -2$) versus the number of epochs E . In panels (a, c, e), we use overlap loss function $\mathcal{L}_{\text{Overlap}}$; in panels (b, d, f), we use \mathcal{L}_{MSE} . In panels (a,b), we vary the batch size B . We vary the number of samples M in panels (c,d); in panels (e,f), we vary the hidden ratio α . If not stated otherwise, the number of training samples is $M = 10^5$, the hidden ratio is $\alpha = 3$, the batch size is $B = 32$ and $\gamma = 10^{-5}$ is the initial learning rate.

of the system, such as the energy, are better represented. We thus study the convergence of a loss function and compare that to the relative energy error \mathcal{E}_r . For the loss function, we evaluate the variance of the loss function σ_{loss} over the past 200 epochs and we plot it against the epoch number. This is because a natural stopping criterion for the optimization is indeed that the variation of the loss function over the epochs is below a certain threshold.

In Figure 6 we show this comparison between the standard deviation of the loss function σ_{loss} over the past 200 epochs, panels (a,b), and the relative energy error \mathcal{E}_r panels (c,d), both versus the number of epochs E . In panels (a,c) we consider the training with the loss function $\mathcal{L}_{\text{Overlap}}$, while in panels

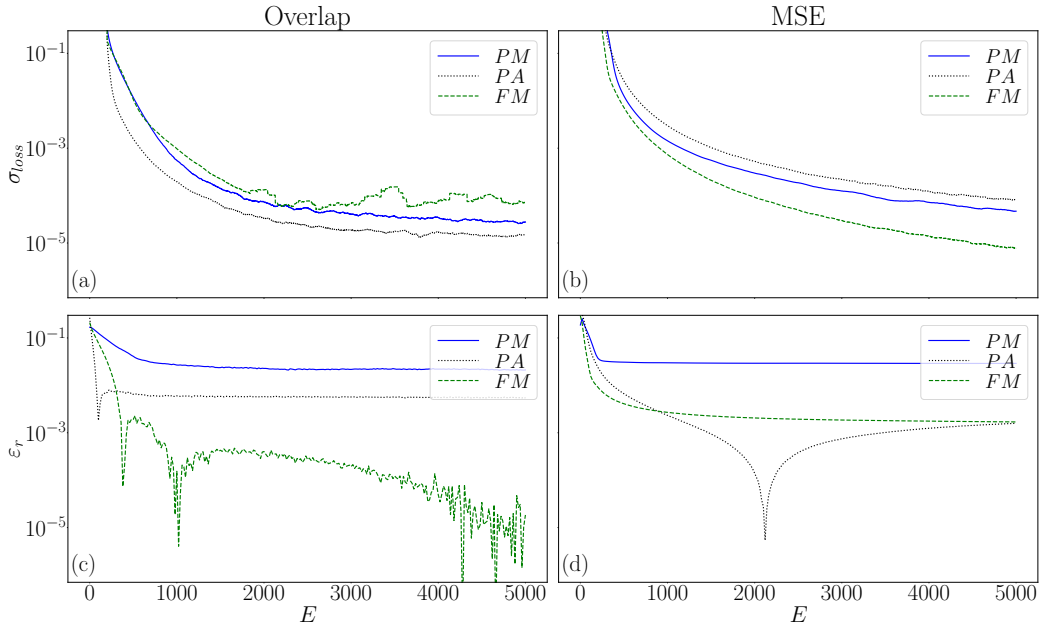


Figure 6: (a,b) Variance of the loss function value σ_{loss} versus number of epochs E . (c,d) Relative energy error \mathcal{E}_r versus the number of epochs E . Panels (a,c) are for $\mathcal{L}_{\text{Overlap}}$, and panels (b,d) are for \mathcal{L}_{MSE} . The blue continuous line is for the paramagnetic (PM) phase $J_1 = 2$ and $J_2 = -1$, the grey dotted line for the pair-antiferromagnetic (PA) phase $J_1 = 1$ and $J_2 = -2$, and the green dashed line for the ferromagnetic (FM) phase $J_1 = 1$ and $J_2 = 2$. In all panels we have used $B = 32$, $M = 10^5$, $\alpha = 3$ and $\gamma = 10^{-5}$.

(b,d) we used the loss function \mathcal{L}_{MSE} . In each panel the blue continuous line corresponds to the paramagnetic phase ($J_1 = 2$ and $J_2 = -1$), the grey dotted line to the pair-antiferromagnetic phase ($J_1 = 1$ and $J_2 = -2$), and the green dashed line to the ferromagnetic phase ($J_1 = 1$ and $J_2 = 2$). We observe that, generally, a decrease in the loss function indeed results in a wave function with energy closer to the ground state energy, however, a quantitative correspondence between the two is not guaranteed.

6. Conclusion

We have studied the supervised training of a neural network to represent the ground state of a many-body quantum system. We considered systems, and their corresponding Hamiltonians, in various phases of matter, namely, the paramagnetic phase, the ferromagnetic phase, and the pair-antiferromagnetic phase. We considered two different loss functions for the

training of the neural network, one that tries to maximize the overlap between the trained data and the neural network wave function, $\mathcal{L}_{\text{Overlap}}$, and one that tries to reduce the difference between the logarithm of the probability amplitudes and the output of the neural network \mathcal{L}_{MSE} .

As possible strategies for supervised learning, we observed that the loss function $\mathcal{L}_{\text{Overlap}}$ generally results in wave functions with more accurate ground state energy in all the phases considered. We associate this performance to the fact that the overlap loss function does not require an exact match of the predicted output with the training data, but instead it can be proportional. This would be relevant also for other types of Hamiltonians. However, it is important that for overlap, the neural network output is rescaled to increase the stability of the algorithm, see Ref. [55] and Appendix A. In our analysis of the hyperparameters, we found that smaller batch sizes result in better performance, but this also requires a larger number of epochs to converge (see Appendix B). Furthermore, larger sample sizes generally help to obtain better results, but larger hidden dimensions can result, especially when using $\mathcal{L}_{\text{Overlap}}$, in overfitting when dealing with relatively simple wave functions.

Further directions include investigating the supervised learning of wave functions that may not be described by real positive numbers, for example, for a more complex ground state, an excited state (but still an eigenstate of the system), or even non-equilibrium states which behave like steady states [73, 74].

7. Acknowledgments

S.B. acknowledges support from the Ministry of Education Singapore, under the grants MOE-T2EP50120-0019 and MOE-T1 251RES2302. D.P. acknowledges support from the Ministry of Education Singapore under the grant MOE-T2EP50120-0019 and the National Research Foundation, Singapore under its QEP2.0 programme (NRF2021-QEP2-02-P03). The computational work for this article was partially performed at the National Supercomputing Centre, Singapore [75]. The codes and data generated are both available upon reasonable request to the authors.

References

- [1] G. Carleo, I. Cirac, K. Cranmer, L. Daudet, M. Schuld, N. Tishby, L. Vogt-Maranto, L. Zdeborová, [Machine learning and the physical sciences](#), Rev. Mod. Phys. 91 (2019) 045002. [doi:10.1103/RevModPhys.](#)

91.045002.

URL <https://link.aps.org/doi/10.1103/RevModPhys.91.045002>

- [2] R. G. Melko, G. Carleo, J. Carrasquilla, J. I. Cirac, [Restricted boltzmann machines in quantum physics](#), Nature Physics 15 (2019) 887. doi:10.1038/s41567-019-0545-1. URL <https://doi.org/10.1038/s41567-019-0545-1>
- [3] J. Carrasquilla, G. Torlai, [How to use neural networks to investigate quantum many-body physics](#), PRX Quantum 2 (2021) 040201. doi:10.1103/PRXQuantum.2.040201. URL <https://link.aps.org/doi/10.1103/PRXQuantum.2.040201>
- [4] J. Biamonte, P. Wittek, N. Pancotti, P. Rebentrost, N. Wiebe, S. Lloyd, [Quantum machine learning](#), Nature 549 (7671) (2017) 195–202. URL <https://www.nature.com/articles/nature23474>
- [5] V. Dunjko, H. J. Briegel, [Machine learning & artificial intelligence in the quantum domain: a review of recent progress](#), Reports on Progress in Physics 81 (7) (2018) 074001. doi:10.1088/1361-6633/aab406. URL <https://dx.doi.org/10.1088/1361-6633/aab406>
- [6] P. Mehta, M. Bukov, C.-H. Wang, A. G. Day, C. Richardson, C. K. Fisher, D. J. Schwab, [A high-bias, low-variance introduction to machine learning for physicists](#), Physics Reports 810 (2019) 1–124, a high-bias, low-variance introduction to Machine Learning for physicists. doi:<https://doi.org/10.1016/j.physrep.2019.03.001>. URL <https://www.sciencedirect.com/science/article/pii/S0370157319300766>
- [7] L. Wang, [Discovering phase transitions with unsupervised learning](#), Phys. Rev. B 94 (2016) 195105. doi:10.1103/PhysRevB.94.195105. URL <https://link.aps.org/doi/10.1103/PhysRevB.94.195105>
- [8] J. Carrasquilla, R. G. Melko, [Machine learning phases of matter](#), Nature Physics 13 (5) (2017) 431–434. URL <https://www.nature.com/articles/nphys4035>
- [9] E. van Nieuwenburg, Y. H. Liu, S. Huber, [Learning phase transitions by confusion](#), Nature Phys 13 (2017) 435. doi:10.1038/nphys4037. URL <https://doi.org/10.1038/nphys4037>

- [10] J. Wei, X.-Y. Sun, K. Xu, H.-X. Deng, J. Chen, Z. Wei, M. Lei, [Machine learning in materials science](#), *InfoMat* 1 (2019) 338. doi:10.1002/inf2.12028.
URL <https://doi.org/10.1002/inf2.12028>
- [11] B. Lanyon, C. Maier, M. Holzäpfel, T. Baumgratz, C. Hempel, P. Jurcevic, I. Dhand, A. S. Buyskikh, A. J. Daley, M. Cramer, M. B. Plenio, R. Blatt, C. F. Roos, [Efficient tomography of a quantum many-body system](#), *Nature Physics* 13 (2017) 1158. doi:10.1038/nphys4244.
URL <https://doi.org/10.1038/nphys4244>
- [12] G. Torlai, G. Mazzola, J. Carrasquilla, M. Troyer, R. Melko, G. Carleo, [Neural-network quantum state tomography](#), *Nature Physics* 14 (5) (2018) 447–450. doi:10.1038/s41567-018-0048-5.
URL <https://doi.org/10.1038/s41567-018-0048-5>
- [13] Q. Xu, S. Xu, [Neural network state estimation for full quantum state tomography](#), arXiv.1811.06654 (2018).
URL <https://doi.org/10.48550/arXiv.1811.06654>
- [14] J. Carrasquilla, G. Torlai, R. G. Melko, L. Aolita, [Reconstructing quantum states with generative models](#), *Nature Machine Intelligence* 1 (2019) 155. doi:10.1038/s42256-019-0028-1.
URL <https://doi.org/10.1038/s42256-019-0028-1>
- [15] T. Westerhout, N. Astrakhantsev, K. S. Tikhonov, M. I. Katsnelson, A. A. Bagrov, [Generalization properties of neural network approximations to frustrated magnet ground states](#), *Nature Communications* 11 (1) (2020) 1593. doi:10.1038/s41467-020-15402-w.
URL <https://doi.org/10.1038/s41467-020-15402-w>
- [16] Y. Quek, S. Fort, H. Ng, [Adaptive quantum state tomography with neural networks](#), *npj Quantum Information* 7 (2021) 105. doi:10.1038/s41534-021-00436-9.
URL <https://doi.org/10.1038/s41534-021-00436-9>
- [17] D. Koutný, L. Motka, Z. c. v. Hradil, J. Řeháček, L. L. Sánchez-Soto, [Neural-network quantum state tomography](#), *Phys. Rev. A* 106 (2022) 012409. doi:10.1103/PhysRevA.106.012409.
URL <https://link.aps.org/doi/10.1103/PhysRevA.106.012409>

- [18] L. Banchi, E. Grant, A. Rocchetto, S. Severini, [Modelling non-markovian quantum processes with recurrent neural networks](#), New Journal of Physics 20 (12) (2018) 123030. doi:10.1088/1367-2630/aaf749.
URL <https://dx.doi.org/10.1088/1367-2630/aaf749>
- [19] C. Guo, K. Modi, D. Poletti, [Tensor-network-based machine learning of non-markovian quantum processes](#), Phys. Rev. A 102 (2020) 062414. doi:10.1103/PhysRevA.102.062414.
URL <https://link.aps.org/doi/10.1103/PhysRevA.102.062414>
- [20] M. Bukov, [Reinforcement learning for autonomous preparation of floquet-engineered states: Inverting the quantum kapitza oscillator](#), Phys. Rev. B 98 (2018) 224305. doi:10.1103/PhysRevB.98.224305.
URL <https://link.aps.org/doi/10.1103/PhysRevB.98.224305>
- [21] M. Bukov, A. G. R. Day, D. Sels, P. Weinberg, A. Polkovnikov, P. Mehta, [Reinforcement learning in different phases of quantum control](#), Phys. Rev. X 8 (2018) 031086. doi:10.1103/PhysRevX.8.031086.
URL <https://link.aps.org/doi/10.1103/PhysRevX.8.031086>
- [22] S. Jerbi, C. Gyurik, S. Marshall, H. Briegel, V. Dunjko, [Parametrized quantum policies for reinforcement learning](#), in: M. Ranzato, A. Beygelzimer, Y. Dauphin, P. Liang, J. W. Vaughan (Eds.), Advances in Neural Information Processing Systems, Vol. 34, Curran Associates, Inc., 2021, pp. 28362–28375.
URL https://proceedings.neurips.cc/paper_files/paper/2021/file/eec96a7f788e88184c0e713456026f3f-Paper.pdf
- [23] D. Burgarth, K. Maruyama, F. Nori, [Coupling strength estimation for spin chains despite restricted access](#), Phys. Rev. A 79 (2009) 020305. doi:10.1103/PhysRevA.79.020305.
URL <https://link.aps.org/doi/10.1103/PhysRevA.79.020305>
- [24] E. Bairey, I. Arad, N. H. Lindner, [Learning a local hamiltonian from local measurements](#), Phys. Rev. Lett. 122 (2019) 020504. doi:10.1103/PhysRevLett.122.020504.
URL <https://link.aps.org/doi/10.1103/PhysRevLett.122.020504>

- [25] X. Ma, Z. C. Tu, S.-J. Ran, [Deep learning quantum states for hamiltonian estimation](#), Chinese Physics Letters 38 (11) (2021) 110301. doi:10.1088/0256-307X/38/11/110301. URL <https://dx.doi.org/10.1088/0256-307X/38/11/110301>
- [26] F. Wilde, A. Kshetrimayum, I. Roth, D. Hangleiter, R. Sweke, J. Eisert, [Scalably learning quantum many-body hamiltonians from dynamical data](#), arXiv:2209.14328 (2022). URL <https://doi.org/10.48550/arXiv.2209.14328>
- [27] T. Xiao, J. Fan, G. Zeng, [Parameter estimation in quantum sensing based on deep reinforcement learning](#), npj Quantum Information 8 (2022) 2. doi:10.1038/s41534-021-00513-z. URL <https://doi.org/10.1038/s41534-021-00513-z>
- [28] E. Bairey, C. Guo, D. Poletti, N. H. Lindner, I. Arad, [Learning the dynamics of open quantum systems from their steady states](#), New Journal of Physics 22 (3) (2020) 032001. doi:10.1088/1367-2630/ab73cd. URL <https://doi.org/10.1088/1367-2630/ab73cd>
- [29] V. Volokitin, I. Meyerov, S. Denisov, [Machine learning approach to the Floquet–Lindbladian problem](#), Chaos: An Interdisciplinary Journal of Nonlinear Science 32 (4), 043117 (04 2022). doi:10.1063/5.0086062. URL <https://doi.org/10.1063/5.0086062>
- [30] G. Carleo, M. Troyer, [Solving the quantum many-body problem with artificial neural networks](#), Science 355 (6325) (2017) 602–606. URL <https://www.science.org/doi/full/10.1126/science.aag2302>
- [31] M. J. Hartmann, G. Carleo, [Neural-network approach to dissipative quantum many-body dynamics](#), Phys. Rev. Lett. 122 (2019) 250502. doi:10.1103/PhysRevLett.122.250502. URL <https://link.aps.org/doi/10.1103/PhysRevLett.122.250502>
- [32] F. Vicentini, A. Biella, N. Regnault, C. Ciuti, [Variational neural-network ansatz for steady states in open quantum systems](#), Phys. Rev. Lett. 122 (2019) 250503. doi:10.1103/PhysRevLett.122.250503.

- URL <https://link.aps.org/doi/10.1103/PhysRevLett.122.250503>
- [33] N. Yoshioka, R. Hamazaki, [Constructing neural stationary states for open quantum many-body systems](#), Phys. Rev. B 99 (2019) 214306. doi:10.1103/PhysRevB.99.214306.
URL <https://link.aps.org/doi/10.1103/PhysRevB.99.214306>
- [34] A. Nagy, V. Savona, [Variational quantum monte carlo method with a neural-network ansatz for open quantum systems](#), Phys. Rev. Lett. 122 (2019) 250501. doi:10.1103/PhysRevLett.122.250501.
URL <https://link.aps.org/doi/10.1103/PhysRevLett.122.250501>
- [35] M. Schmitt, M. Heyl, [Quantum many-body dynamics in two dimensions with artificial neural networks](#), Physical Review Letters 125 (10) (2020) 100503.
URL <https://journals.aps.org/prl/abstract/10.1103/PhysRevLett.125.100503>
- [36] I. L. Gutiérrez, C. B. Mendl, [Real time evolution with neural-network quantum states](#), Quantum 6 (2022) 627. doi:10.22331/q-2022-01-20-627.
URL <https://doi.org/10.22331/q-2022-01-20-627>
- [37] Y. Nomura, [Helping restricted boltzmann machines with quantum-state representation by restoring symmetry](#), Journal of Physics: Condensed Matter 33 (17) (2021) 174003. doi:10.1088/1361-648x/abe268.
URL <https://doi.org/10.1088/1361-648x/abe268>
- [38] C.-Y. Park, M. J. Kastoryano, [Expressive power of complex-valued restricted boltzmann machines for solving non-stoquastic hamiltonians](#), arXiv:2012.08889 (2020).
URL <https://arxiv.org/abs/2012.08889>
- [39] C.-Y. Park, M. J. Kastoryano, [Geometry of learning neural quantum states](#), Phys. Rev. Research 2 (2020) 023232. doi:10.1103/PhysRevResearch.2.023232.
URL <https://link.aps.org/doi/10.1103/PhysRevResearch.2.023232>

- [40] K. Choo, G. Carleo, N. Regnault, T. Neupert, [Symmetries and many-body excitations with neural-network quantum states](#), Phys. Rev. Lett. 121 (2018) 167204. doi:10.1103/PhysRevLett.121.167204.
URL <https://link.aps.org/doi/10.1103/PhysRevLett.121.167204>
- [41] R. Zen, L. My, R. Tan, F. Hébert, M. Gattobigio, C. Miniatura, D. Poletti, S. Bressan, [Transfer learning for scalability of neural-network quantum states](#), Phys. Rev. E 101 (2020) 053301. doi:10.1103/PhysRevE.101.053301.
URL <https://link.aps.org/doi/10.1103/PhysRevE.101.053301>
- [42] R. Zen, L. My, R. Tan, F. Hébert, M. Gattobigio, C. Miniatura, D. Poletti, S. Bressan, [Finding quantum critical points with neural-network quantum states](#), in: G. D. Giacomo, A. Catalá, B. Dilkina, M. Milano, S. Barro, A. Bugarín, J. Lang (Eds.), ECAI 2020 - 24th European Conference on Artificial Intelligence, 29 August-8 September 2020, Santiago de Compostela, Spain, August 29 - September 8, 2020 - Including 10th Conference on Prestigious Applications of Artificial Intelligence (PAIS 2020), Vol. 325 of Frontiers in Artificial Intelligence and Applications, IOS Press, 2020, pp. 1962–1969. doi:10.3233/FAIA200315.
URL <https://doi.org/10.3233/FAIA200315>
- [43] C. Roth, A. H. MacDonald, [Group convolutional neural networks improve quantum state accuracy](#), arXiv:2104.05085 (2021).
URL <https://arxiv.org/abs/2104.05085>
- [44] D. Kochkov, B. K. Clark, [Variational optimization in the ai era: Computational graph states and supervised wave-function optimization](#), arXiv:1811.12423 (2018).
URL <https://arxiv.org/abs/1811.12423>
- [45] R. Verdel, M. Schmitt, Y.-P. Huang, P. Karpov, M. Heyl, [Variational classical networks for dynamics in interacting quantum matter](#), Phys. Rev. B 103 (2021) 165103. doi:10.1103/PhysRevB.103.165103.
URL <https://link.aps.org/doi/10.1103/PhysRevB.103.165103>
- [46] K. Donatella, Z. Denis, A. L. Boité, C. Ciuti, [Dynamics with autoregressive neural quantum states: application to critical quench dynamics](#),

- arxiv:2209.03241 (2022). doi:10.48550/arXiv.2209.03241.
URL <https://doi.org/10.48550/arXiv.2209.03241>
- [47] B. Jónsson, B. Bauer, G. Carleo, [Neural-network states for the classical simulation of quantum computing](#), arxiv:1808.05232 (2018). doi:10.48550/arXiv.1808.05232.
URL <https://doi.org/10.48550/arXiv.1808.05232>
- [48] M. Medvidović, G. Carleo, [Classical variational simulation of the quantum approximate optimization algorithm](#), npj Quantum Inf 7 (2021) 101. doi:10.1038/s41534-021-00440-z.
URL <https://doi.org/10.1038/s41534-021-00440-z>
- [49] A. Sinibaldi, C. Giuliani, G. Carleo, F. Vicentini, [Unbiasing time-dependent variational monte carlo by projected quantum evolution](#), arxiv:2305.14294 (2023). doi:10.48550/arXiv.2305.14294.
URL <https://doi.org/10.48550/arXiv.2305.14294>
- [50] D. Kim, D.-H. Kim, [Smallest neural network to learn the ising criticality](#), Phys. Rev. E 98 (2018) 022138. doi:10.1103/PhysRevE.98.022138.
URL <https://link.aps.org/doi/10.1103/PhysRevE.98.022138>
- [51] S. Efthymiou, M. J. S. Beach, R. G. Melko, [Super-resolving the ising model with convolutional neural networks](#), Phys. Rev. B 99 (2019) 075113. doi:10.1103/PhysRevB.99.075113.
URL <https://link.aps.org/doi/10.1103/PhysRevB.99.075113>
- [52] F. D'Angelo, L. Böttcher, [Learning the ising model with generative neural networks](#), Phys. Rev. Res. 2 (2020) 023266. doi:10.1103/PhysRevResearch.2.023266.
URL <https://link.aps.org/doi/10.1103/PhysRevResearch.2.023266>
- [53] S. Sorella, M. Casula, D. Rocca, [Weak binding between two aromatic rings: Feeling the van der waals attraction by quantum monte carlo methods](#), The Journal of chemical physics 127 (1) (2007) 014105.
URL <https://aip.scitation.org/doi/10.1063/1.2746035>
- [54] W. Zhang, X. Xu, Z. Wu, V. Balachandran, D. Poletti, [Ground state search by local and sequential updates of neural network quantum states](#),

- Phys. Rev. B 107 (2023) 165149. doi:10.1103/PhysRevB.107.165149.
URL <https://link.aps.org/doi/10.1103/PhysRevB.107.165149>
- [55] F. Vicentini, D. Hofmann, A. Szabó, D. Wu, C. Roth, C. Giuliani, G. Pescia, J. Nys, V. Vargas-Calderon, N. Astrakhantsev, G. Carleo, [Netket 3: Machine learning toolbox for many-body quantum systems](#), arXiv:2112.10526 (2021).
URL <https://arxiv.org/abs/2112.10526>
- [56] A. I. Larkin, Y. N. Ovchinnikov, [Quasiclassical method in the theory of superconductivity](#), Soviet Journal of Experimental and Theoretical Physics 28 (1969) 1200.
URL <http://jetp.ras.ru/cgi-bin/e/index/e/28/6/p1200?a=list>
- [57] U. Schollwöck, The density-matrix renormalization group in the age of matrix product states, Annals of physics 326 (1) (2011) 96–192.
- [58] A. L. Maas, A. Y. Hannun, A. Y. Ng, et al., [Rectifier nonlinearities improve neural network acoustic models](#), Proc. ICML 30 (1) (2013) 3.
URL https://ai.stanford.edu/~amaas/papers/relu_hybrid_icml2013_final.pdf
- [59] Z.-Y. Han, J. Wang, H. Fan, L. Wang, P. Zhang, [Unsupervised generative modeling using matrix product states](#), Phys. Rev. X 8 (2018) 031012. doi:10.1103/PhysRevX.8.031012.
URL <https://link.aps.org/doi/10.1103/PhysRevX.8.031012>
- [60] H. Peres Casagrande, B. Xing, M. Dalmonte, A. Rodriguez, V. Balachandran, D. Poletti, [Complexity of spin configurations dynamics due to unitary evolution and periodic projective measurements](#), arxiv.org:2305.03334.
URL <https://arxiv.org/abs/2305.03334>
- [61] H. P. Casagrande, [Dmrg ground-state search and sampling data](#) (2023).
URL <https://github.com/heitorc7/NNQSupervisedLearningDMRG>
- [62] N. Metropolis, A. Rosenbluth, M. Rosenbluth, A. Teller, E. Teller, [Equation of state calculations by fast computing machines](#), Journal of Chemical Physics 21 (1953) 1087. doi:10.1063/1.1699114.
URL <http://dx.doi.org/10.1063/1.1699114>

- [63] W. Hastings, [Monte carlo sampling methods using markov chains and their applications](#), *Biometrika* 57 (1970) 97. doi:[10.1093/biomet/57.1.97](https://doi.org/10.1093/biomet/57.1.97).
URL <https://doi.org/10.1093/biomet/57.1.97>
- [64] Z. Cai, J. Liu, [Approximating quantum many-body wave functions using artificial neural networks](#), *Physical Review B* 97 (3) (2018) 035116.
URL <https://journals.aps.org/prb/abstract/10.1103/PhysRevB.97.035116>
- [65] D. P. Kingma, J. Ba, [Adam: A method for stochastic optimization](#), [arxiv.org:1412.6980](https://arxiv.org/abs/1412.6980) (2017).
URL <https://arxiv.org/abs/1412.6980>
- [66] U. Schollwöck, [The density-matrix renormalization group in the age of matrix product states](#), *Annals of Phys.* 326 (2011) 96–192. doi:[10.1016/j.aop.2010.09.012](https://doi.org/10.1016/j.aop.2010.09.012).
URL <https://link.aps.org/doi/10.1016/j.aop.2010.09.012>
- [67] M. Fishman, S. R. White, E. M. Stoudenmire, [The ITensor software library for tensor network calculations](#), [arXiv:2007.14822](https://arxiv.org/abs/2007.14822) (2020).
URL <https://arxiv.org/abs/2007.14822>
- [68] H. P. Casagrande, D. Poletti, G. T. Landi, [Analysis of a density matrix renormalization group approach for transport in open quantum systems](#), *Computer Physics Communications* 267 (2021) 108060. doi:<https://doi.org/10.1016/j.cpc.2021.108060>.
URL <https://www.sciencedirect.com/science/article/pii/S0010465521001727>
- [69] G. Carleo, K. Choo, D. Hofmann, J. E. Smith, T. Westerhout, F. Alet, E. J. Davis, S. Efthymiou, I. Glasser, S.-H. Lin, et al., [Netket: A machine learning toolkit for many-body quantum systems](#), *SoftwareX* 10 (2019) 100311.
- [70] J. Bradbury, R. Frostig, P. Hawkins, M. J. Johnson, C. Leary, D. Maclaurin, G. Necula, A. Paszke, J. VanderPlas, S. Wanderman-Milne, Q. Zhang, [JAX: composable transformations of Python+NumPy](#)

- programs (2018).
URL <http://github.com/google/jax>
- [71] M. Abadi, A. Agarwal, P. Barham, E. Brevdo, Z. Chen, C. Citro, G. S. Corrado, A. Davis, J. Dean, M. Devin, S. Ghemawat, I. Goodfellow, A. Harp, G. Irving, M. Isard, Y. Jia, R. Jozefowicz, L. Kaiser, M. Kudlur, J. Levenberg, D. Mané, R. Monga, S. Moore, D. Murray, C. Olah, M. Schuster, J. Shlens, B. Steiner, I. Sutskever, K. Talwar, P. Tucker, V. Vanhoucke, V. Vasudevan, F. Viégas, O. Vinyals, P. Warden, M. Wattemberg, M. Wicke, Y. Yu, X. Zheng, [TensorFlow: Large-scale machine learning on heterogeneous systems](#), software available from tensorflow.org (2015).
URL <https://www.tensorflow.org/>
- [72] J. Zhang, Y. Zhang, Y. Lu, A comparative study of deep learning frameworks based on short-term power load forecasting experiments, in: Journal of Physics: Conference Series, Vol. 2005, IOP Publishing, 2021, p. 012070.
- [73] X. Xu, C. Guo, D. Poletti, [Typicality of nonequilibrium quasi-steady currents](#), Phys. Rev. A 105 (2022) L040203. doi:10.1103/PhysRevA.105.L040203.
URL <https://link.aps.org/doi/10.1103/PhysRevA.105.L040203>
- [74] X. Xu, C. Guo, D. Poletti, [Emergence of steady currents due to strong prethermalization](#), Phys. Rev. A 107 (2023) 022220. doi:10.1103/PhysRevA.107.022220.
URL <https://link.aps.org/doi/10.1103/PhysRevA.107.022220>
- [75] The computational work for this article was partially performed on resources of the National Supercomputing Centre, Singapore, <https://www.nscg.sg/>.

Appendix A. Not rescaled wave function for overlap KL divergence loss functions

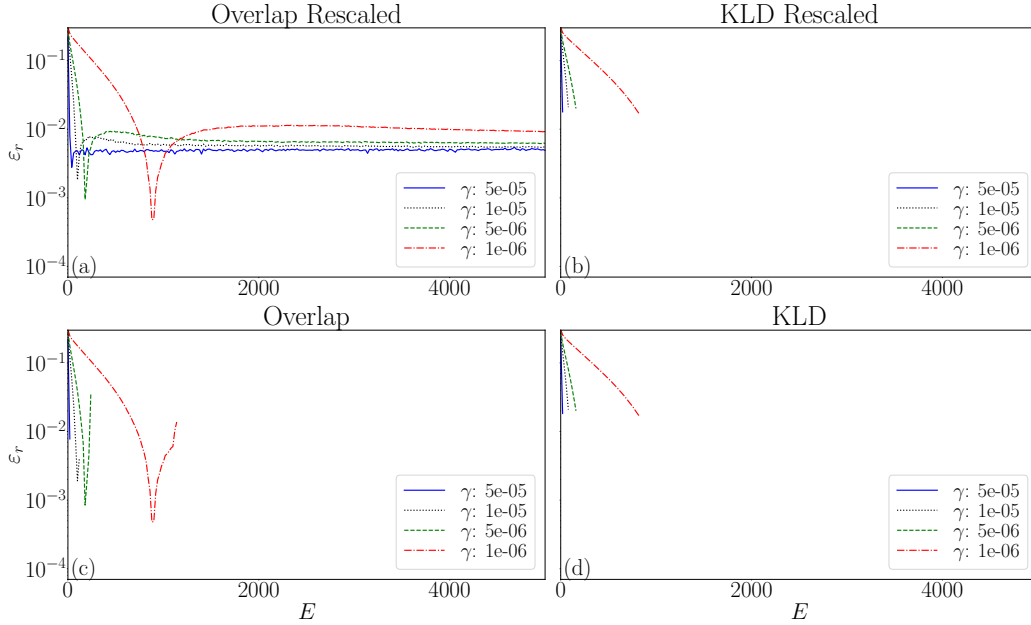


Figure A1: Relative error \mathcal{E}_r for the pair-antiferromagnetic ground state ($J_1 = 1$ and $J_2 = -2$) versus number of epochs E . (a) is the rescaled version of overlap. (b) is the rescaled version of KL divergence. (c) is the original overlap and (d) is the original KL divergence. We vary to different learning rates compared to the control/default value $\gamma = 10^{-5}$ in the paper. the number of training sample is $M = 10^5$, batch size $B = 32$, and the hidden ratio is $\alpha = 3$.

In the main portion of the article, when using $\mathcal{L}_{\text{Overlap}}$, we rescale the neural network output using Equation (3). Here we show that if we were not to do this, the training would be more unstable and it could lead to the network parameters becoming NaN. This is a general result, as we show by discussing two loss functions, the overlap loss function $\mathcal{L}_{\text{Overlap}}$ and the Kullback–Leibler (KL) divergence. In this work, the loss function for KL divergence is given by Equation (A.1).

$$\mathcal{L}_{\text{KLD}}(\Psi_G, \Psi) = \sum_{m=1}^{M_u} |\Psi_G(\mathbf{x}_m)|^2 \ln \left(\frac{|\Psi_G(\mathbf{x}_m)|^2}{|\Psi(\mathbf{x}_m)|^2} \right) \quad (\text{A.1})$$

where the wave functions could be rescaled, i.e. each one is divided by the maximum value obtained over the M_u unique samples, or not. Our results are

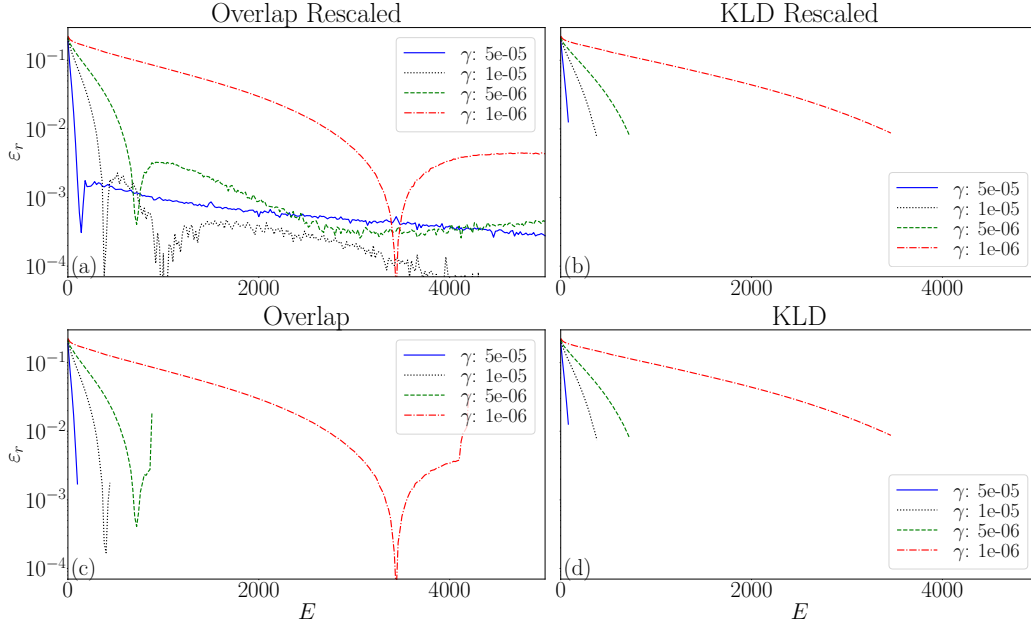


Figure A2: Relative error \mathcal{E}_r for the ferromagnetic ground state ($J_1 = 1$ and $J_2 = 2$) versus number of epochs E . (a) is the rescaled version of overlap. (b) is the rescaled version of KL divergence. (c) is the original overlap and (d) is the original KL divergence. We vary to different learning rates compared to the control/default value $\gamma = 10^{-5}$ in the paper. the number of training sample is $M = 10^5$, batch size $B = 32$, and the hidden ratio is $\alpha = 3$.

shown in Figure A1 and Figure A2, respectively for parameters such that the ground state is in the pair-antiferromagnetic and in the ferromagnetic phase (the paramagnetic phase is more stable). In the figures, an interrupted line before 5000 epochs signifies that the training leads to NaN for the network parameters. Importantly, we note that even using a rescaled neural network for the KL divergence loss function can result in instability of the learning dynamics, as shown by the interruption of the lines. We associate the instability of the KL divergence loss function to the highly peaked distributions that we are using for the training.

In general, however, we note that using a smaller initial learning rate γ results in a delayed instability of the neural network parameters' dynamics.

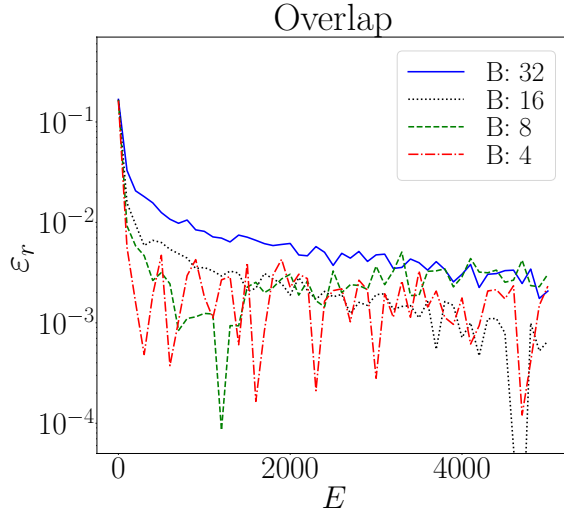


Figure A3: Relative error \mathcal{E}_r for the paramagnetic ground state ($J_1 = 2$ and $J_2 = -1$) versus number of epochs E . we use overlap loss function $\mathcal{L}_{\text{Overlap}}$ and vary to smaller batch size compared to the control/default value $B = 32$ in the paper. The number of the training samples is $M = 10^5$, the learning rate is 10^{-4} and the hidden ratio is $\alpha = 3$.

Appendix B. Smaller batch size for training

In the main portion of the article, we have observed that the smaller the batch size the better the wave function approaches the ground state energy. Here we explore this further with even smaller batch sizes using $\mathcal{L}_{\text{Overlap}}$ as a loss function. In Figure A3 we show results for 128 spins in the paramagnetic phase versus the number of epochs. We observe that smaller batch sizes can result in larger oscillations and not significant improvements while, not shown, requiring more time. For these reasons, we kept $B = 32$ as a standard minimum value for the computations in the main portion of the article. We highlight here that for Figure A3 we have used an initial learning rate $\gamma = 10^{-4}$ which, for $\mathcal{L}_{\text{Overlap}}$ and in the paramagnetic phase, allows us to reach energies closer to the ground state than using $\gamma = 10^{-5}$. The overall dependence on the batch size B is qualitatively similar for the two values of learning rate γ .

Appendix C. About the Mapalus

In MAPALUS, users can use neural-network quantum states to find the ground state or excited states of a given system. The system is described by the structure and the quantum model of the system. The library non-exclusively readily contains the implementation for the transverse field Ising model, the Heisenberg XYZ model, and the Heisenberg J1-J2 model. Users can choose to train a neural-network quantum states in either an unsupervised or a supervised manner with different neural network architectures (the library currently contains the code for multilayer feed forward neural network, restricted Boltzmann machines, and deep Boltzmann machines) with dynamic and static stopping criteria, and different Monte Carlo sampling algorithms. The library also provides a logging mechanism that saves the necessary information from the training. The logging process also includes the computation of observables. MAPALUS is written in Python with TENSORFLOW. It is easily customizable and runs in parallel on Message Passing Interface or general-purpose graphics processing units.

Using MAPALUS, we only needed to implement the different loss functions considered in order to empirically explore the respective effectiveness of the different configurations and parameters' values of the supervised multi-layer feed forward neural network quantum states.